First Steps of Retinal Photoisomerization in Proteorhodopsin

Martin O. Lenz,* Robert Huber,* Bernhard Schmidt,† Peter Gilch,† Rolf Kalmbach,‡ Martin Engelhard,‡ and Josef Wachtveitl*

*Institut für Physikalische und Theoretische Chemie, Johann-Wolfgang-Goethe-Universität, Frankfurt, Germany; †Universität München, Department für Physik, Lehrstuhl für BioMolekulare Optik, Munich, Germany; and ‡Max-Planck-Institute of Molecular Physiology, Department of Physical Biochemistry, Dortmund, Germany

ABSTRACT The early steps (<1 ns) in the photocycle of the detergent solubilized proton pump proteorhodopsin are analyzed by ultrafast spectroscopic techniques. A comparison to the first primary events in reconstituted proteorhodopsin as well as to the well known archaeal proton pump bacteriorhodopsin is given. A dynamic Stokes shift observed in fs-time-resolved fluorescence experiments allows a direct observation of early motions on the excited state potential energy surface. The initial dynamics is dominated by sequentially emerging stretching (<150 fs) and torsional (~300 fs) modes of the retinal. The different protonation states of the primary proton acceptor Asp-97 drastically affect the reaction rate and the overall quantum efficiencies of the isomerization reactions, mainly evidenced for time scales above 1 ps. However, no major influence on the fast time scales (~150 fs) could be seen, indicating that the movement out of the Franck-Condon region is fairly robust to electrostatic changes in the retinal binding pocket. Based on fs-time-resolved absorption and fluorescence spectra, ground and exited state contributions can be disentangled and allow to construct a reaction model that consistently explains pH-dependent effects in solubilized and reconstituted proteorhodopsin.

INTRODUCTION

Since the membrane protein proteorhodopsin (PR) as a new member of type I retinal binding protein family was discovered in uncultivated marine *γ-proteobacteria*, interest rose concerning its potential relevance in an unknown phototrophic pathway in the ocean's photic zone (1–3). Analog to bacteriorhodopsin (BR), PR was shown to work as a light-driven proton pump. Thus, also *γ-proteobacteria* might use this proton gradient across the membrane for energy requirements such as ATP synthesis. After photoexcitation PR undergoes a photocycle forming a series of distinguishable spectroscopic intermediates (K, M, N, and O) (4–8). During this photocycle (turnover time 20 ms) a proton is transported from the cytoplasmatic to the extracellular side of the membrane. In comparison to BR most of the residues involved in the vectorial proton transport are conserved (9). The primary proton acceptor Asp-85 in BR corresponds to Asp-97 in PR, as well as the counterion of the protonated Schiff base Arg-82, Asp-212, and Lys-216 to Arg-94, Asp-227, and Lys-231 in PR. The primary proton donor Asp-96 is replaced by Glu-108 in PR (1). However, PR seems to lack some ionizable residues which in BR are involved in the fast proton release at the extracellular side (1,10–12).

The pK_a of the primary proton acceptor Asp-97 is unusually high and lies at neutral pH ~7.6. Thus it is shifted around 5 units to higher pH-values in comparison to the homologous amino acid Asp-85 of BR ($pK_a = 2.5$). Therefore, spectroscopic and electrophysiological characterization of PR is much easier than in BR and other retinal proteins. In fact, there is good evidence that for PR the proton pumping direction is inversed below the pK_a of Asp-97 (6), which would allow the bacteria to regulate their membrane potential in a more subtle manner. Although pH-dependent photocurrent measurements on planar lipid bilayers and voltage-clamp experiments of *Xenopus laevis* oocytes expressing PR clearly showed bidirectional H^+-transport, no H^+-transport could be determined in different studies using photoelectric current measurements at acidic conditions (7,13).

The key event of the early steps within the photocycle is the isomerization of the covalently bound retinal. Upon illumination an all-*trans* to 13-*cis* isomerization takes place. As has been determined by retinal extraction in Friedrich et al. (6), before illumination (dark-adapted state) the configuration is mainly all-*trans* (80%) and changes to 60% for light-adapted PR under alkaline conditions. For acidic conditions no light/dark adaptation could be seen and 80% of PR can be found in the all-*trans* conformation (6). However, in recent studies employing FTIR-spectroscopy it has been reported that almost no spectral changes appear upon light/dark adaptation (14) and that the retinal exists only in the all-*trans* conformation for the dark-adapted state (15). This is underlined by recent results from solid-state NMR-spectroscopy on PR (16).

Some models have been proposed for the photocycle of PR based on different spectroscopic investigations (4–8) and most of them agree in principle with the photocycle model established for BR (17,18). The photoreaction starts in the first excited state of the all-*trans* retinal. According to quantum mechanical calculations the propagation along the first excited state PES involves a retinal stretching as well as a torsional motion around the C13-C14 double bond, leading

Submitted September 19, 2005, and accepted for publication March 22, 2006.

Address reprint requests to Josef Wachtveitl, E-mail: wveitl@theochem.uni-frankfurt.de.

0006-3495/06/07/255/08 $2.00

doi: 10.1529/biophysj.105.074690

to a conical intersection of the S_0 and S_1 energy surfaces at a 90° twisted geometry (19–22). On the ground state surface the path splits up, either back to the all-*trans* or toward the 13-*cis* configuration (K-intermediate).

For several different retinal proteins primary photodynamics have been investigated in different surroundings. It was shown that spectroscopic characteristics of retinal as well as dynamics of isomerization have been strongly influenced by the environment. Although this spectral tuning is essential for the function of some retinal proteins, details of the tuning mechanisms within the protein microenvironment are still only partially understood and subject of ongoing discussions (23–28).

Here, we provide evidence for electrostatic control of reaction pathways of solubilized PR samples during the first 1000 ps after photoexcitation. Transient absorption measurements with ~100 fs time resolution as well as transient fluorescent measurements have been performed on PR under different conditions. In continuation of our earlier work (29), we will focus on the following aspects. First, the influence of the protonation state of the primary proton acceptor on the very early events in the photocycle (<500 fs) can now be addressed in detail. The additional time-resolved fluorescence measurements open the possibility to observe fast excited-state dynamics without superimposed ground state contributions. Second, this investigation allows to evaluate solubilization effects (solubilized versus reconstituted) on the primary dynamics of this integral membrane protein. Based on these results a reaction model can be worked out, where the influence of alternate deactivation pathways after photoexcitation of PR will be taken into account, leading to a consistent description of pH-dependent photodynamics.

MATERIAL AND METHODS

Sample preparation

Expression and purification of PR in *Escherichia coli* membranes was performed as described in Friedrich et al. (6). The purified PR in 0.5 M NaCl, 20 mM Tris pH 8.0, 0.1% (w/v) dodecylmaltoside was adjusted to the appropriate pH by adding 1 M NaOH or HCl and concentrated in a Centriprep centrifugal filter (10 kD, Millipore). For the spectroscopic measurements the protein concentration was 5 mg/ml, which was calculated from the retinal absorption using a molar extinction coefficient of 45,000 M^{-1} cm^{-1} (6).

Stationary measurements

Absorption spectra were recorded with an Analytik Jena (Jena, Germany) S100 spectrometer using 1-mm fused silica cuvettes and corrected for light scattering. Fluorescence measurements were performed with a commercial fluorimeter (Varian, Cary Eclipse, Australia) or within the setup for time-resolved fluorescence measurements. Fluorescence spectra of 1-amino-anthraquinone measured under the same experimental conditions served as a standard. The radiative lifetime was determined using the Strickler-Berg relationship (30). Although not all conditions for applying this relation to PR are fulfilled, it has been shown by Kochendoerfer et al. (31) that valuable information can be gained for retinal proteins nevertheless.

Time-resolved spectroscopy

The time-resolved measurements using femtosecond pump/probe technique were performed using a Clark CPA 2001 (Dexter, MI) laser/amplifier system operating at a repetition rate of ~1 kHz and at a central wavelength of 775 nm. The pulse width of the system was ~150 fs (FWHM). The laser served as pulse source for the following nonlinear processes. Excitation pulses were generated using a noncollinear optical parametric amplifier (NOPA) (32) centered at a wavelength of 525 nm and focused to a diameter of 100 μm inside the sample. The pulse length was compressed down to 50 fs, typical pulse energies were around 50 nJ, small enough to prevent multi-photon excitation of the sample. The sample was probed with single filament white light (supercontinuum) pulses generated in a 2-mm CaF_2 plate (33), whereby a spectral range of 380–730 nm was used for probing. The continuum pulses were dispersed by two VIS-spectrometers (sample and reference), and recorded with two 42-segment diode arrays. Data acquisition was performed in single shot detection mode as balanced and referenced measurement providing signal/noise ratios up to 10^4 (29). Excitation and probe pulses were polarized parallel. To account for long-term drifts and possible degradation of the sample, the ratio between probe and reference signals for the nonexcited sample was determined every third shot.

A continuous exchange of the sample between successive laser shots was achieved by using a flow cuvette (path length 0.5 mm) and a syringe pump. This prevents multiple excitation of molecules within their photocycle and accumulation of potentially degraded photoproducts. The Kerr gate setup for the femtosecond fluorescence experiments is detailed in Schmidt et al. (34). Particulars on an analogous experiment on BR are given in Schmidt et al. (35). The pertinent parameters for the fs-fluorescence setup were the following. Laser pulses stemming from a Clark CPA 2001 system were converted to 525 nm using a NOPA. Pulses with an energy of ~150 nJ and a duration of ~40 fs were focused to a diameter of ~160 μm into the sample cell. This translates into an excitation density below 0.4 photons per molecule. As shown in Schmidt et al. (35), for BR, nonlinear effects of the excitation can be excluded at this density. The absorbance at the excitation wavelength in the 1-mm flow cell was ~0.5 OD. Sample volumes of a few ml were circulated at a speed sufficient to exchange the excited volume in between laser shots. At each setting of the delay line the fluorescence signal was accumulated for 2 s and the results of eight delay scans were averaged. To correct the spectral dependence of time zero, the procedure as described in Schmidt et al. (35) has been used.

RESULTS AND DISCUSSION

Spectroscopic properties

The absorption spectrum of PR responds to a pH change (Fig. 1): for pH 6.4, which is below the pK_a of the primary proton acceptor Asp-97 (6), a maximum at 531 nm is observed, whereas at pH 9 the peak is located at 521 nm. Similar shifts for PR have been reported before (36). In contrast to the absorption spectra neither a shift nor a change in the shape of the emission spectra could be seen. The excitation maximum is centered around 565 nm (for emission at 710 nm) and the emission maximum is located at 700 nm (see Fig. 1) indicating a pronounced Stokes shift of ~170 nm (~4500 cm^{-1}), typical for a large reorganization energy as found in many isomerizing molecules and pointing to a distinct conformational change on the potential energy surface (PES) of the excited state toward a minimum already at this stage. Furthermore Fig. 2 gives an overview of the spectro-temporal behavior of PR upon femtosecond excitation and

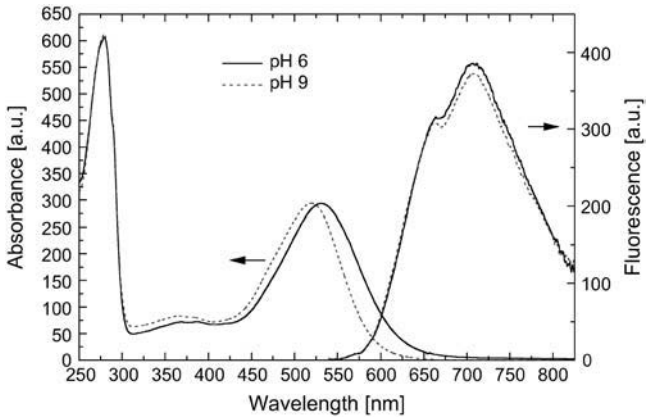

FIGURE 1 Comparison of stationary absorption and fluorescence spectra of proteorhodopsin at pH 6 and at pH 9. pH 6 samples showed stronger scattering and have been corrected for this by subtracting $a + b\lambda^{-4}$ curve.

highlights the pH-dependence of the photodynamics. Four different regions can be discriminated for both samples:

Centered around 470 nm, a dominant positive transient absorption can be identified for PR in both surroundings from the delay time zero up to ~10 ps (see Fig. 2, areas termed *A*). This spectrally fairly broad signature rises within the experimental response time and can be assigned to the absorption of the excited state S_1. It can be observed, that the S_1-decay for the system at pH 6.4 proceeds systematically

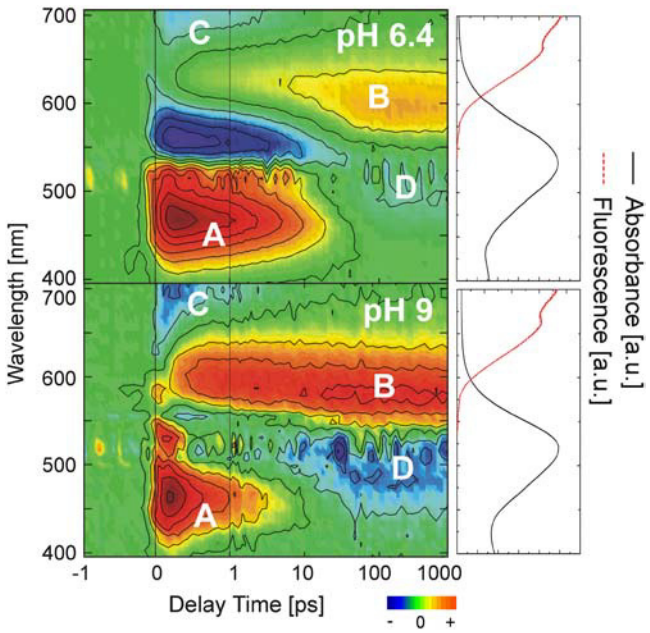

FIGURE 2 (*Left*) Temporal evolution of a light/dark difference absorption of PR at pH 6.4 and pH 9 (multi-channel detection) after excitation with a 525-nm pulse. Signal amplitudes are color coded: red indicates positive, green zero, and blue indicates negative absorbance changes. The scale is linear for $\tau < 1$ ps and logarithmic for longer delay times. (*Right*) Absorption and corresponding fluorescence spectra of different PR samples.

slower than the one at pH 9. A detailed comparison of the involved time constants will be given below.

The areas in the contour spectra termed *B* show a positive contribution persisting until more than 1 ns, which show the same spectral characteristics and can thus be attributed to the K-intermediate as reported in Friedrich et al. (6) for nanosecond measurements. Qualitative and quantitative good agreement can be found comparing the transient difference absorption at maximum delay time of 1000 ps with the ones reported in the abovementioned reference. This intermediate absorbing around 1 ns is the product state for the primary reaction investigated here and contains the isomerized retinal in the ground state. The relative amplitude of the described signal with regard to the excited state absorption or the ground state bleach (see next paragraph) should scale with the quantum efficiency of the whole isomerization process. However, a comparison of the quantum efficiencies at different pH-values only holds true for the assumption of similar extinctions for all contributing species. An exact consideration of this effect is difficult, since spectral characteristics of, e.g., the pure excited state absorption or the K-intermediate are not known, but based on the known pH-dependence of absorption ($\Delta\lambda \approx 10$ nm) and fluorescence spectra ($\Delta\lambda \approx 0$ nm) these shifts should not completely account for the observed differences in quantum efficiency.

The negative transient absorbance change for wavelengths $\geq$650 nm (*C*) is due to stimulated emission from the excited state. At later delay times this contribution is congested by the superposition of the absorption of the product state. At a probe wavelength of 700 nm this congestion is not so severe and the emission signal is best probed here (or via time-resolved fluorescence). The negative transient absorption for wavelengths $\leq$500 nm at longer delay times ($\tau > 50$ ps) can be assigned to the bleaching signal of the ground state (*D*). For delay times <50 ps, this effect is overcompensated by excited state absorption, so that the bleach is clearly visible only for longer delay times.

To analyze the data more quantitatively Fig. 3 shows transients for selected probing wavelengths for acidic and alkaline conditions. At the blue side of the main absorption band (443 nm), an instantaneous increase of the absorbance change can be seen for PR samples at both pH-values characteristic for the build up of the excited state, usually displaying a broad absorption spectrum. This increase decays from hundreds of fs to tens of ps for pH 9 and a long-lasting negative absorbance change due to ground state bleach remains. For pH 6.4 the excited state is depopulated on the low ps timescale, also there a long-lasting negative absorbance change persists. It is obvious that signals are changing significantly faster in the case of alkaline pH. This can also be seen in the transient spectra (Fig. 4), where nearly no positive absorption remains after 5 ps for alkaline PR, whereas a strong absorption change is still present for the acidic form.

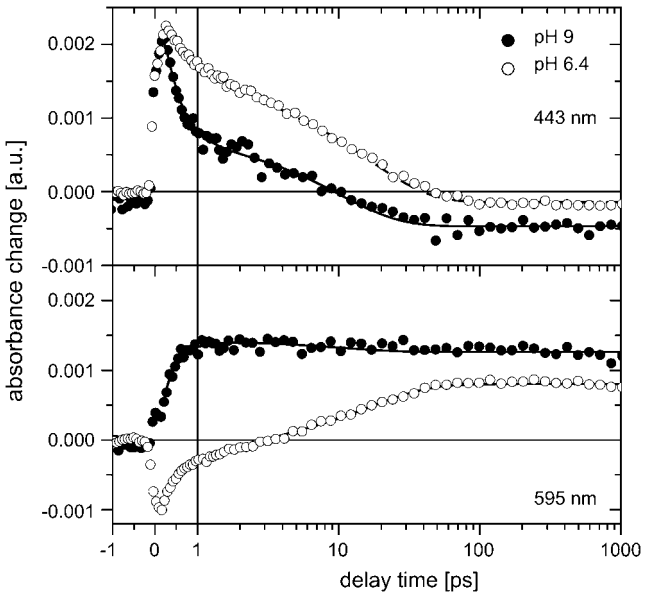

FIGURE 3 Comparison of transient absorbance changes of PR at acidic and alkaline pH at different probing wavelengths. Solid lines represent results of a multi-exponential global fit analysis of the complete data set.

Functional ultrafast dynamics of PR

Although for both samples a ground state bleach, as well as the photoproduct absorption at long delay times, is visible, the absolute values of absorbance changes differ significantly, indicating different amounts of created photoproduct. For pH 9 the bleaching signal and the signal of the K-intermediate at long delay times is approximately twice as high as for pH 6.4. This observation might be attributed to reduced overlap of the absorption spectrum of the K-intermediate and the spectroscopic ground state of the corresponding PR species. However, the overall conserved spectral form as well as the stronger bleach signal in the blue spectral region for pH 9 point more toward a changed quantum efficiency of retinal isomerization. We can therefore conclude that up to 1 ns twice as much molecules end up in the photoproduct state and do not return to the all-*trans*-ground state for alkaline pH than under acidic conditions. This supports the model, that, if the primary proton acceptor is deprotonated, the protein will undergo its normal photocycle in contrast to the situation when the Asp-97 is protonated and the isomerization of the retinal is slowed down.

At the red side of the main absorption band (595 nm) a significantly different behavior of the protein in different surroundings can be seen. For a pH value of 9 a strong increase in the absorbance change is obvious. The increase grows with a time constant of a few hundred fs followed by a minor decay in the 10 ps regime (Fig. 3). A constant positive absorbance remains for longer delay times up to 1 ns. Under more acidic conditions (pH = 6.4) an initial decrease can be seen, but the transient absorption signal changes sign after a few ps and exhibits a positive absorbance change for delay

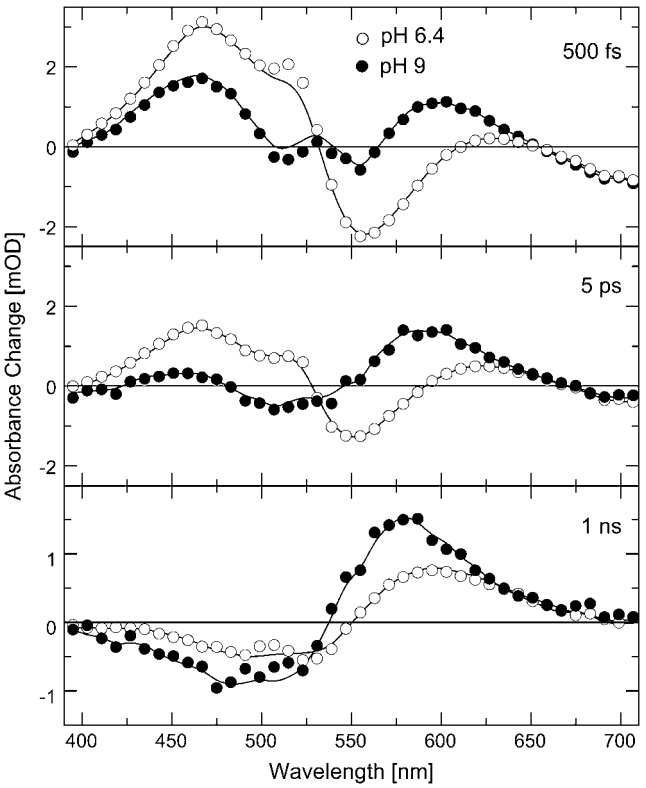

FIGURE 4 Transient spectra at different delay times for PR at pH 6.4 and pH 9. Almost no excited state absorption remains for pH 9 for delay times longer than 5 ps. The more pronounced ground state bleach as well as the stronger absorption of the K-intermediate is apparent for pH 9 at 1 ns.

times up to 1 ns. The rise of this positive signal is bi-exponential with time constants of 1 and 16 ps. As reported by Friedrich et al. (6) the photoproduct of the initial reaction of PR should be present around 570 nm. It becomes clear from the transients, that for pH 9 the photoproduct builds up within a couple of hundreds of fs followed by some minor changes, whereas for pH 6.4 for short delay times the transients are dominated by the bleach of the ground state and the product state absorption grows in with time constants of 1 ps and 16 ps.

The 40-time traces have been fitted with a global-fitting routine, which assumes exponential decays with equal time constants for all wavelengths. The data can satisfactorily be fitted with four time-constants for PR at both pH-values (Table 1). To indicate that principal processes and time constants are similar for solubilized and reconstituted PR, time constants are also given for reconstituted PR according to Huber et al. (29). It is evident that the general trend of the slowing down of nearly all processes upon decreasing pH is conserved also for the solubilized PR samples. Ultrafast kinetics below 200 fs are described by the first time constant for both pH values ($\tau_{1(\mathrm{pH6.4})} = 150$ fs, $\tau_{1(\mathrm{pH9})} = 140$ fs). As can be seen from time-resolved fluorescent data, a dynamic Stokes shift (35) (see below) is present in the spectroscopic data, so the ultrashort time constant represents a mixture of

TABLE 1 Comparison of time constants derived by a global exponential fit analysis of transient absorption data for different PR samples

	τ_1 [ps]	τ_2 [ps]	τ_3 [ps]	τ_4 [ps]
PR (pH 6.4) solubilized	0.15	1.0	16.2	∞
PR (pH 6) reconstituted (29)	<0.2	0.7	15	∞
PR (pH 9) solubilized	0.14	0.28	9.5	∞
PR (pH 9) reconstituted (29)	<0.2	0.4	8	∞

For completeness, data from literature are given as well.

very different contributions, which strictly cannot be described by one exponential decay. Furthermore, if the ultrashort time constants are similar they might influence each other leading to unphysical spectra. Because τ_1 and τ_2 are close to each other for pH 9 and partially compensate each other, only the sum of these two decay associated spectra is given (Fig. 5, *bottom*). This can be interpreted in terms of a fit with three exponential decays, however three time constants are not sufficient to describe all spectral features accurately especially for the very short times so nonetheless four time constants have to be taken into account. Spectral features for τ_2 and τ_3 are closely resemble each other, indicating that the underlying processes are related. The amplitude for the slowest decay shows not only the bleached ground state, but also the photoproduct (early K-type) can be identified. For BR it is reported that the first ground-state intermediate converts with a time constant of 3 ps to the K-intermediate (37). For solubilized PR the quality of the global fit was not improved by introducing another time constant, therefore no statement can be given regarding this transition.

Since transient absorbance experiments probe ground state dynamics as well as excited state dynamics and signals are partially overlapping, it is quite difficult to distinguish between the two of them. Therefore time-resolved fluorescence spectroscopy has also been applied to investigate the early photodynamics of PR at pH 8. A short-lived and spectrally broad (580–850 nm) fluorescence signal can be seen after excitation at 525 nm (Fig. 6). The data can be modeled with four time constants ($\tau_1 \sim 0.05$–0.15 ps, $\tau_2 \sim 0.45$ ps, $\tau_3 \sim 4$ ps and $\tau_4 = \infty$,) where τ_1, τ_2, and τ_3 describe sample dynamics and τ_4 a possible long time offset. The former values are in good agreement with the results obtained from fitting only the transient absorbance data in the region above 650 nm (region *C*), where stimulated emission signals should be present. What can be clearly seen from the overview graph is a wavelength dependent time zero. This dynamic Stokes shift (35) on the order of 50–150 fs can be attributed to a movement on the excited state surface out of the Franck-Condon region and agrees with the fastest time constant observed in the transient absorbance measurements as well as with a dynamic Stokes-shift observed for BR (35).

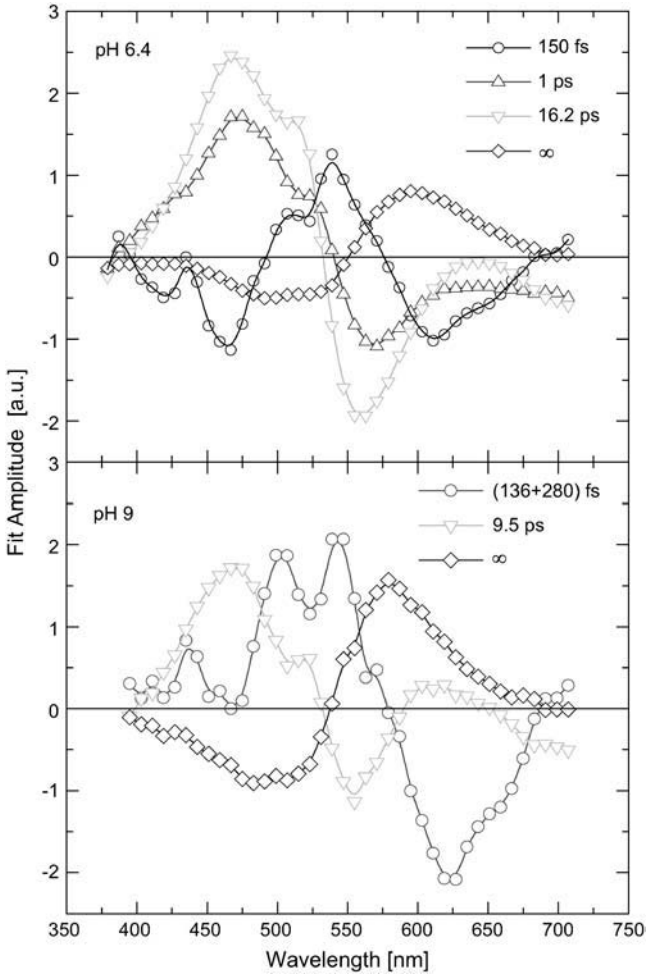

FIGURE 5 Decay associated spectra of the multi-exponential global fit analysis of PR at pH 6.4 and pH 9. For the acidic sample, decay associated spectra for all four time constants are given. The sum of the spectra of the first two time constants and individual spectra for the longer time constants are given for the alkaline pH. See text for details.

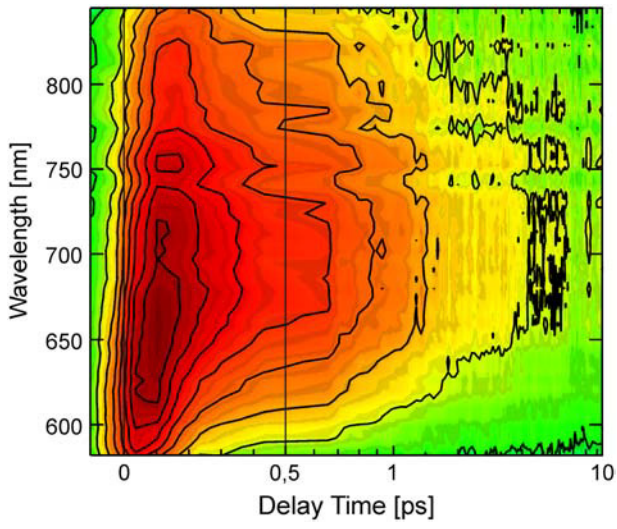

FIGURE 6 Time-resolved fluorescence measurements of PR at pH 8. A dynamic Stokes shift as well as a broad and short-lived fluorescence is clearly visible.

Analysis of the amplitude spectra (decay associated spectra of fluorescence, not shown) shows that the spectral characteristics for τ_2 and τ_3 constants are very similar and therefore two similar decay channels out of the S_1-state are likely, which agrees with results from the transient absorption experiments where τ_2 and τ_3 showed similar spectral characteristics also.

Based on a fluorescence quantum yield of PR of 2.6×10^{-4} and a radiative lifetime of 6 ns deduced from a Strickler-Berg analysis one obtains a fluorescence lifetime of 1.4 ps. The value is in good agreement with the averaged fluorescence lifetime measured in the Kerr gate experiment. This indicates that no long-lived excited state contributes to the steady state fluorescence emission, an observation which is further underlined when comparing the steady state emission spectrum with a numerical integration of the time-resolved experiment (Fig. 7).

Directly after excitation a positive absorbance change around 450 nm builds up for PR samples for both pH values and decays with $\tau_1 \approx 150$ fs. This signal is part of the excited state dynamics of the retinal in PR. These early processes are manifested in the fluorescence experiment as dynamic Stokes shift and a rapid decay which can be attributed to the movement out of the Franck-Condon region. For BR the molecular picture developed for this movement is an in-plane stretching vibration of the conjugated carbon chain of the retinal initiating the isomerization reaction. In contrast to the pH-dependence of the longer time constants, no indication could be found that the initial stretching mode is influenced by the protonation state of Asp-97. According to Abramczyk (38), this initial stretching in retinal proteins is then followed by a torsional motion (around the C13-C14 double bond for PR), which takes place on the order of 300 fs to 1 ps depending on the protonation state of the primary proton acceptor. In agreement with results from reconstituted PR this corresponds to a fast transition to the ground state, via a conical intersection. The states decaying with longer time constants τ_2 and τ_3 are not identical to the original Franck-Condon states but exhibit similar amplitude spectra indicating, that the initial and final states of these transitions are very similar. Since biphasic behavior has also been reported for other retinal proteins like halorhodopsin (39) this PR feature is not unique. Comparing the relation of the amplitudes for both pH values indicates, that for pH 6.4 the slower decay channel (16.2 ps) is favored, whereas for the alkaline pH the faster decay channel (300 fs) is preferred. Sample heterogeneity might be the reason for the biphasic behavior. (29) However, since recent investigations show that the dark-adapted state mainly consists of all-*trans* retinal (14–16), PR with different retinal isomers appears unlikely as the main cause of multi-exponential decay. Instead, a branched reaction model explains the observed behavior. An energy and reaction model of the primary reaction of PR (time constants for pH 9), which takes all observed features into account, is given in Fig. 8. After photoexcitation into the Franck-Condon region mainly two nuclear coordinates play a role. A nuclear stretch on the order of 150 fs followed by a torsional motion on the order of 300 fs lead to a conical intersection with the ground state. Although most molecules decay along this pathway, some will not reach the CI directly, but end up in a state on the S_1 potential energy surface separated from the CI by an energetic barrier. They can access the CI within some picoseconds and proceed on the lower surface either back to an all-*trans* configuration or to the 13-*cis* state (K-intermediate).

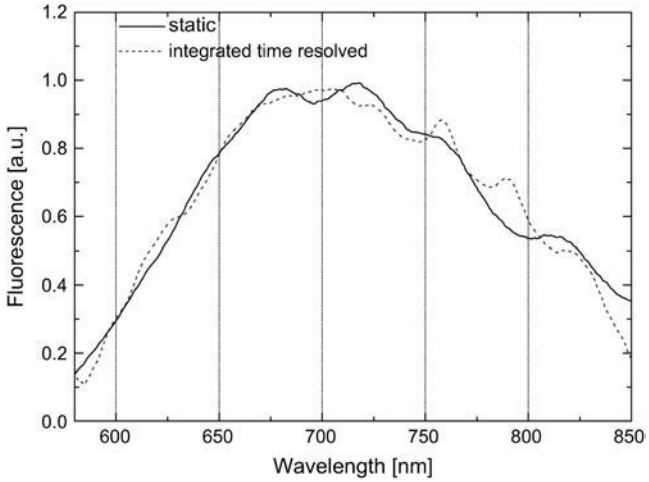

FIGURE 7 Comparison of static and integrated time-resolved fluorescence data. Good agreement between these data is obvious indicating no other processes than the observed ones contributing to the static fluorescence. The wiggles stem from an interference filter introduced in the fluorescence setup to block remaining unconverted light from the upconversion process.

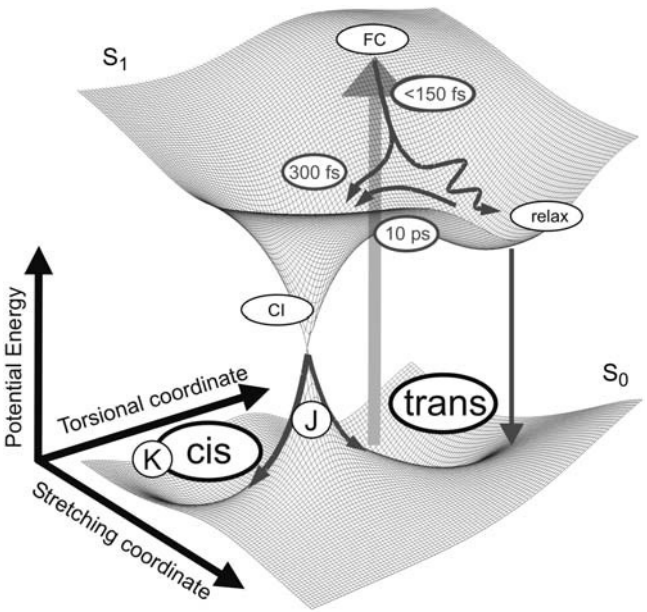

FIGURE 8 Proposed reaction model for the primary events in PR.

In agreement with results obtained for reconstituted samples all longer time constants are considerably slowed down as the pH is lowered. Since the first excited state exhibits ionic character in comparison to the electronic ground state, partial positive charge is moved toward the hydrocarbon tail of the retinal upon excitation. This positive charge is then in turn stabilized by the negatively charged residue Asp-97 near the C13 position leading to a decreased double bond character at this position, which results in lowered energy for the torsional motion. This is reflected in an increased reaction rate (40) and agrees with observations on partially mutated archaeal rhodopsins with uncharged residues at the position of the primary proton acceptor (39). Another possible explanation which is supported by findings in recent publications (41,42) might be charge translocation and weakening of all double bonds of the chromophore. Due to the counterion close to the C13 position, this bond is especially affected and thus isomerization might take place at this position. The protonation of the primary proton acceptor can be visualized as a tilting of the S_1 surface leading to different amount of molecules ending up in the faster or slower decay channel (a few 100 fs versus a few ps). Reaction rates definitely change, but as pH-dependent static fluorescence measurements indicate, the fluorescence maximum is not changing, showing that the position of the ''relaxed'' S_1-state in terms of reaction coordinates as origin for the fluorescence is unaltered.

CONCLUDING REMARKS

The light-induced dynamics in photoactive biomolecules is not only of fundamental importance for understanding the coupling between light absorption and protein conformational changes which triggers the biological function of the particular chromoprotein. A comprehensive knowledge can also be utilized for design and development of biomimetic light-driven Z/E (*cis*/*trans*) switches (43). Furthermore, protonated Schiff bases may provide model compounds for molecular devices or motors. Therefore studying and controlling reaction pathways on the femtosecond level is of fundamental importance. The observation of an unusual high pK_a of the primary proton acceptor offers the possibility to use this molecular switch in a rather common environment and controlling its properties by only slightly changing the pH.

The authors thank E. Bamberg for initiating this project and for many helpful discussions.

This work was supported by DFG SFB 472 (''Molecular Bioenergetics'').

REFERENCES

1. Beja, O., L. Aravind, E. V. Koonin, M. T. Suzuki, A. Hadd, L. P. Nguyen, S. Jovanovich, C. M. Gates, R. A. Feldman, J. L. Spudich, E. N. Spudich, and E. F. DeLong. 2000. Bacterial rhodopsin: evidence for a new type of phototrophy in the sea. *Science*. 289:1902–1906.
2. Beja, O., E. N. Spudich, J. L. Spudich, M. Leclerc, and E. F. DeLong. 2001. Proteorhodopsin phototrophy in the ocean. *Nature*. 411:786–789.
3. Venter, J. C., K. Remington, J. F. Heidelberg, A. L. Halpern, D. Rusch, J. A. Eisen, D. Y. Wu, I. Paulsen, K. E. Nelson, W. Nelson, D. E. Fouts, S. Levy, A. H. Knap, M. W. Lomas, K. Nealson, O. White, J. Peterson, J. Hoffman, R. Parsons, H. Baden-Tillson, C. Pfannkoch, Y. H. Rogers, and H. O. Smith. 2004. Environmental genome shotgun sequencing of the Sargasso Sea. *Science*. 304:66–74.
4. Lakatos, M., J. K. Lanyi, J. Szakacs, and G. Varo. 2003. The photochemical reaction cycle of proteorhodopsin at low pH. *Biophys. J.* 84:3252–3256.
5. Krebs, R. A., U. Alexiev, R. Partha, A. DeVita, and M. S. Braiman. 2002. Detection of fast light-activated H^+ release and M intermediate formation from proteorhodopsin. *BMC Physiol.* 2:5–13.
6. Friedrich, T., S. Geibel, R. Kalmbach, I. Chizhov, K. Ataka, J. Heberle, M. Engelhard, and E. Bamberg. 2002. Proteorhodopsin is a light-driven proton pump with variable vectoriality. *J. Mol. Biol.* 321:821–838.
7. Dioumaev, A. K., J. M. Wang, Z. Balint, G. Varo, and J. K. Lanyi. 2003. Proton transport by proteorhodopsin requires that the retinal Schiff base counterion Asp-97 be anionic. *Biochemistry*. 42:6582–6587.
8. Varo, G., L. S. Brown, M. Lakatos, and J. K. Lanyi. 2003. Characterization of the photochemical reaction cycle of proteorhodopsin. *Biophys. J.* 84:1202–1207.
9. Krebs, R. A., D. Dunmire, R. Partha, and M. S. Braiman. 2003. Resonance Raman characterization of proteorhodopsin's chromophore environment. *J. Phys. Chem. B*. 107:7877–7883.
10. Dioumaev, A. K., H. T. Richter, L. S. Brown, M. Tanio, S. Tuzi, H. Saito, Y. Kimura, R. Needleman, and J. K. Lanyi. 1998. Existence of a proton transfer chain in bacteriorhodopsin: participation of Glu-194 in the release of protons to the extracellular surface. *Biochemistry*. 37:2496–2506.
11. Balashov, S. P., E. S. Imasheva, T. G. Ebrey, N. Chen, D. R. Menick, and R. K. Crouch. 1997. Glutamate-194 to cysteine mutation inhibits fast light-induced proton release in bacteriorhodopsin. *Biochemistry*. 36:8671–8676.
12. Brown, L. S., J. Sasaki, H. Kandori, A. Maeda, R. Needleman, and J. K. Lanyi. 1995. Glutamic-acid-204 is the terminal proton release group at the extracellular surface of bacteriorhodopsin. *J. Biol. Chem.* 270: 27122–27126.
13. Sineshchekov, O. A., and J. L. Spudich. 2004. Light-induced intramolecular charge movements in microbial rhodopsins in intact *E. coli* cells. *Photochem. Photobiol. Sci.* 3:548–554.
14. Bergo, V., J. J. Amsden, E. N. Spudich, J. L. Spudich, and K. J. Rothschild. 2004. Structural changes in the photoactive site of proteorhodopsin during the primary photoreaction. *Biochemistry*. 43: 9075–9083.
15. Imasheva, E. S., K. Shimono, S. P. Balashov, J. M. Wang, U. Zadok, M. Sheves, N. Kamo, and J. K. Lanyi. 2005. Formation of a long-lived photoproduct with a deprotonated Schiff base in proteorhodopsin, and its enhancement by mutation of Asp-227. *Biochemistry*. 44:10828–10838.
16. Lorch, M. S. S., I. Weber, and C. Glaubitz. 2005. Photocycle of proterhodopsin investigated by solid state NMR. GDCh Magnetic Resonance Division, 27th Discussion Meeting. Mainz, Germany.
17. Haupts, U., J. Tittor, and D. Oesterhelt. 1999. Closing in on bacteriorhodopsin: progress in understanding the molecule. *Annu. Rev. Biophys. Biomol. Struct.* 28:367–399.
18. Lanyi, J. K. 2000. Molecular mechanism of ion transport in bacteriorhodopsin: insights from crystallographic, spectroscopic, kinetic, and mutational studies. *J. Phys. Chem. B*. 104:11441–11448.
19. Song, L., and M. A. El-Sayed. 1998. Primary step in bacteriorhodopsin photosynthesis: bond stretch rather than angle twist of its retinal excited-state structure. *J. Am. Chem. Soc*. 120:8889–8890.

20. Garavelli, M., P. Celani, F. Bernardi, M. A. Robb, and M. Olivucci. 1997. The $C_5H_6NH^{2+}$ protonated Shiff base: an ab initio minimal model for retinal photoisomerization. *J. Am. Chem. Soc.* 119:6891–6901.

21. Gonzalez-Luque, R., M. Garavelli, F. Bernardi, M. Merchan, M. A. Robb, and M. Olivucci. 2000. Computational evidence in favor of a two-state, two-mode model of the retinal chromophore photoisomerization. *Proc. Natl. Acad. Sci. USA.* 97:9379–9384.

22. De Vico, L., C. S. Page, M. Garavelli, F. Bernardi, R. Basosi, and M. Olivucci. 2002. Reaction path analysis of the ''tunable'' photoisomerization selectivity of free and locked retinal chromophores. *J. Am. Chem. Soc.* 124:4124–4134.

23. De Vico, L., M. Garavelli, F. Bernardi, and M. Olivucci. 2005. Photoisomerization mechanism of 11-*cis*-locked artificial retinal chromophores: Acceleration and primary photoproduct assignment. *J. Am. Chem. Soc.* 127:2433–2442.

24. Cembran, A., F. Bernardi, M. Olivucci, and M. Garavelli. 2005. The retinal chromophore/chloride ion pair: structure of the photo isomerization path and interplay of charge transfer and covalent states. *Proc. Natl. Acad. Sci. USA.* 102:6255–6260.

25. Cembran, A., F. Bernardi, M. Garavelli, L. Gagliardi, and G. Orlandi. 2004. On the mechanism of the cis-trans isomerization in the lowest electronic states of azobenzene: S-0, S-1, and T-1. *J. Am. Chem. Soc.* 126:3234–3243.

26. Cembran, A., F. Bernardi, M. Olivucci, and M. Garavelli. 2004. Counterion controlled photoisomerization of retinal chromophore models: a computational investigation. *J. Am. Chem. Soc.* 126:16018–16037.

27. Gagliardi, L., G. Orlandi, F. Bernardi, A. Cembran, and M. Garavelli. 2004. A theoretical study of the lowest electronic states of azobenzene: the role of torsion coordinate in the *cis-trans* photoisomerization. *Theor. Chem. Acc.* 111:363–372.

28. Cembran, A., R. Gonzalez-Luque, P. Altoe, M. Merchan, F. Bernardi, M. Olivucci, and M. Garavelli. 2005. Structure, spectroscopy, and spectral tuning of the gas-phase retinal chromophore: the beta-ionone ''handle'' and alkyl group effect. *J. Phys. Chem. A.* 109:6597–6605.

29. Huber, R., T. Köhler, M. O. Lenz, E. Bamberg, R. Kalmbach, M. Engelhard, and J. Wachtveitl. 2005. pH-dependent photoisomerization of retinal in proteorhodopsin. *Biochemistry.* 44:1800–1806.

30. Strickler, S. J., and R. A. Berg. 1962. Relationship between absorption intensity and fluorescence lifetime of molecules. *J. Chem. Phys.* 37: 814–820.

31. Kochendoerfer, G. G., and R. A. Mathies. 1996. Spontaneous emission study of the femtosecond isomerization dynamics of rhodopsin. *J. Phys. Chem.* 100:14526–14532.

32. Wilhelm, T., J. Piel, and E. Riedle. 1997. Sub-20-fs pulses tunable across the visible from a blue-pumped single-pass noncollinear parametric converter. *Opt. Lett.* 22:1494–1496.

33. Huber, R., H. Satzger, W. Zinth, and J. Wachtveitl. 2001. Noncollinear optical parametric amplifiers with output parameters improved by the application of a white light continuum generated in CaF2. *Opt. Commun.* 194:443–448.

34. Schmidt, B., S. Laimgruber, W. Zinth, and P. Gilch. 2003. A broadband Kerr shutter for femtosecond fluorescence spectroscopy. *Appl. Phys. B-Lasers O.* 76:809–814.

35. Schmidt, B., C. Sobotta, B. Heinz, S. Laimgruber, M. Braun, and P. Gilch. 2005. Excited-state dynamics of bacteriorhodopsin probed by broadband femtosecond fluorescence spectroscopy. *Biochim. Biophys. Acta.* 1706:165–173.

36. Imasheva, E. S., S. P. Balashov, J. M. Wang, A. K. Dioumaev, and J. K. Lanyi. 2004. Selectivity of retinal photoisomerization in proteorhodopsin is controlled by aspartic acid 227. *Biochemistry.* 43:1648–1655.

37. Herbst, J., K. Heyne, and R. Diller. 2002. Femtosecond infrared spectroscopy of bacteriorhodopsin chromophore isomerization. *Science.* 297:822–825.

38. Abramczyk, H. 2004. Femtosecond primary events in bacteriorhodopsin and its retinal modified analogs: revision of commonly accepted interpretation of electronic spectra of transient intermediates in the bacteriorhodopsin photocycle. *J. Chem. Phys.* 120:11120–11132.

39. Lutz, I., A. Sieg, A. A. Wegener, M. Engelhard, I. Boche, M. Otsuka, D. Oesterhelt, J. Wachtveitl, and W. Zinth. 2001. Primary reactions of sensory rhodopsins. *Proc. Natl. Acad. Sci. USA.* 98:962–967.

40. Song, L., M. A. El-Sayed, and J. K. Lanyi. 1993. Protein catalysis of the retinal subpicosecond photoisomerization in the primary process of bacteriorhodopsin photosynthesis. *Science.* 261:891–894.

41. Groma, G. I., A. Colonna, J. C. Lambry, J. W. Petrich, G. Varo, M. Joffre, M. H. Vos, and J. L. Martin. 2004. Resonant optical rectification in bacteriorhodopsin. *Proc. Natl. Acad. Sci. USA.* 101: 7971–7975.

42. Schenkl, S., F. van Mourik, G. van der Zwan, S. Haacke, and M. Chergui. 2005. Probing the ultrafast charge translocation of photoexcited retinal in bacteriorhodopsin. *Science.* 309:917–920.

43. Sampedro, D., A. Migani, A. Pepi, E. Busi, R. Basosi, L. Latterini, F. Elisei, S. Fusi, F. Ponticelli, V. Zanirato, and M. Olivucci. 2004. Design and photochemical characterization of a biomimetic light-driven Z/E switcher. *J. Am. Chem. Soc.* 126:9349–9359.